In Situ Image Segmentation Using the Convexity of Illumination Distribution of the Light Sources

Li Zhang

Abstract—When separating objects from a background in an image, we often meet difficulties in obtaining the precise output due to the unclear edges of the objects, as well as the poor or nonuniform illumination. In order to solve this problem, this paper presents an in situ segmentation method that takes advantage of the distribution feature of illumination of light sources, rather than analyzing the image pixels themselves. After analyzing the convexity of illumination distribution (CID) of point and linear light sources, the paper makes use of the CID features to find pixels belonging to the background. Then, some background pixels are selected as control points to reconstruct the image background by means of B-spline; finally, by subtracting the reconstructed background from the original image, global thresholding can be employed to make the final segmentation. Quantitative evaluation experiments are made to test the performance of the method.

Index Terms—Image segmentation, B-spline, illumination, convexity, thresholding.

1 Introduction

In a variety of applications involving visual inspection, it is required to separate objects from the background in an image that is captured under conditions of poor and nonuniform illumination [1]. For example, Fig. 1a is an image taken by a CCD camera in the quantitative evaluation of thin-layer chromatography (TLC) that needs to separate all five of the spots precisely from the background for quantitative evaluation. These kinds of images usually have darker objects against a brighter background or vice versa.

Thresholding is usually the method to solve this kind of problem because a bimodal histogram would often be obtained from an image with objects on the same background. Among global thresholding methods, Otsu's method [2] was tested to be the most efficient one [3]. However, this technique is not suitable for images with uneven background or poor illumination, as shown in Fig. 1c, where the histogram is not bimodal.

It would be wiser to divide the original image into subimages if the histogram of the original image is not bimodal. However, there would still be some subimages that do not have bimodal histograms yet. Chow and Kaneko [4] suggested that if subimages do not have bimodal histograms, their thresholds should be computed by value interpolating from their neighbors. Nakagava and Rosenfeld [5] did some experiments to test Chow and Kaneko's method in a wider application. Fernando and Monro [6] also put forward a local thresholding method in their research which employs the entropy thresholding technique presented by Pun [7] to determine the threshold for each of the subimages. This approach is practical for images with a great change in background. However, if most of the subimages do not have bimodal histograms, such as in Fig. 1a, the segmentation result becomes poor too. Dawound and Kamel [8] also proposed a subimage binarization method that uses the multimodels to iteratively arrive at the optimal threshold for each subimage. This method is only good for document image segmentation where objects have a statistical model. Huang et al. [9] tried to find the perfect threshold for each subimage by changing their sizes. In their method, the threshold for each subimage still employs Otsu's method.

Yanowitz and Bruckstein [1] proposed a different solution. They took the points with the high gradient to be the key points that are thought to be the edge points and combined the points that satisfy the Laplace equation to make a threshold surface. Yanowitz and Bruckstein's method is good for images in which an object has a clear edge. However, it is not suitable for images having objects with unclear edges, as Fig. 1b implies.

Chan et al. [10] proposed an adaptive thresholding approach viewed as the variational translation of Yanowitz and Bruckstein's algorithm. The main advantage of their method is object boundary points selection involving many parameter decisions and interpolations by solving a Laplace equation. It is evident that a distinct object boundary is also a prerequisite in this approach.

Blayvas et al. [11] followed the footsteps of Yanowitz and Bruckstein to use image values at the high gradient points to construct a thresholding surface too. This

• *The author is with the Institute of Image and Computer Graphics, Department of Electronic Engineering, Tsinghua University, Beijing 100084, China. E-mail: chinazhangli@tsinghua.edu.cn.*

Manuscript received 3 Jan. 2007; revised 10 July 2007; accepted 1 Nov. 2007; published online 21 Nov. 2007.
Recommended for acceptance by G. Finlayson.
For information on obtaining reprints of this article, please send e-mail to: tpami@computer.org, and reference IEEECS Log Number TPAMI-0003-0107.
Digital Object Identifier no. 10.1109/TPAMI.2007.70830.

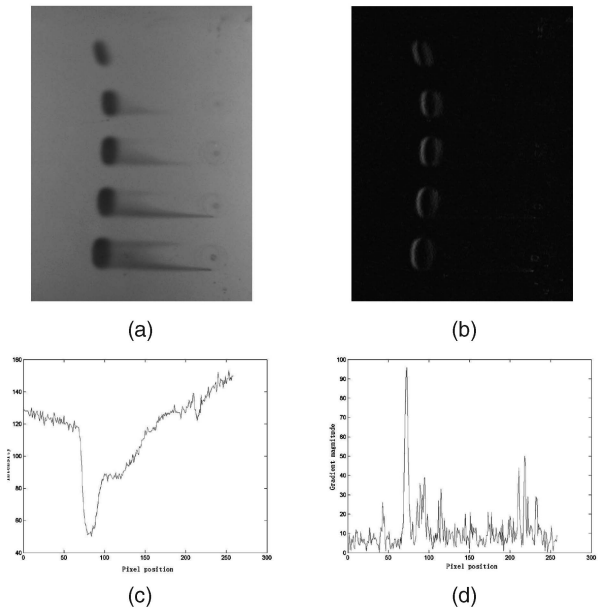

Fig. 1. An image containing objects with unclear edges against a nonuniform background. (a) Original. (b) Sobel gradient. (c) Profile of one scan line of (a). (d) Profile of the corresponding line in (b).

approach is robust to noise. However, the original surface constructed by this method is not continuous, which needs to be modified later. Liu et al. [12] have addressed this issue by making a modification to Yanowitz and Bruckstein's method by setting a surface that is parallel to the background to be the thresholding surface. Their consideration achieved a more concordant thresholding surface to the original image background. However, it does not perform well either when dealing with images whose object's edge is unclear because the support points are still obtained in the same way that Yanowitz and Bruckstein did.

Kim et al. [13] proposed a water flow model method to find the local adaptive thresholding for document image binarization. Oh et al. [14] made an improvement to Kim et al.'s method by taking into account the pixel's gradient magnitude. Their methods are quite good for document image processing, but, when used for the separation of objects with unclear edges on a nonuniform background, as shown in Fig. 1c, it is hard to determine the amount of rainfall.

Wada et al. [15] and Tan et al. [16] had proposed methods based on a shape-from-shading (SFS) method [17] to recover warped book images whose background is uneven. They used a scanner to scan unfolded books aligned on the scanning plane so that the center line separating the book pages is parallel to the scanner's linear light source. Thus, the brightest point on a scan line could be taken as a background point because the illumination intensity at each point on this scan line is almost the same. After reconstructing the shape of the background based on those points using SFS, they could use it to restore the distorted scanner image based on the shape. However, if the uneven background is caused by the nonuniform illumination, it is difficult to find which pixels belong to the background only by their intensity.

From the above-mentioned previous work, we notice that there has not been a method to suit our task of precisely separating objects with unclear edges from an uneven or nonuniform background. As more and more applications of computer vision need to work in situ, taking into account the features of light sources becomes possible and will make the segmentation easier. Therefore, inspired by the thresholding methods mentioned above, this paper aims to reconstruct the image background based on the distribution features of illumination of light sources and then make the segmentation.

The remainder of the paper is organized as follows: Section 2 analyzes the convex and concave distributions of point and linear light sources. In Section 3, we describe in detail how to use those distribution features to reconstruct the nonuniform background. Section 4 evaluates the performance of the proposed method quantitatively. Finally, we present conclusions in Section 5.

2 Convexity of Illumination Distribution

Light plays an important role in the formation of images. When a beam of light strikes a surface of an object, it will be absorbed, reflected, or transmitted. It is the reflected or transmitted light that makes the object visible. The character of the light reflected from or transmitted through the surface of the object depends upon the composition, direction, and geometry of the light source, the surface orientation, and the surface properties of the object [18]. We will analyze the convexity of illumination distribution (CID) of point and linear light sources on a plane and then apply it to in situ image segmentation.

2.1 Convexity of Illumination Distribution of a Point Light Source

Point light is the most popular light model and the basis for other light sources.

Suppose a point light source is above the plane, as shown in Fig. 2a. O is the projection point of the point light

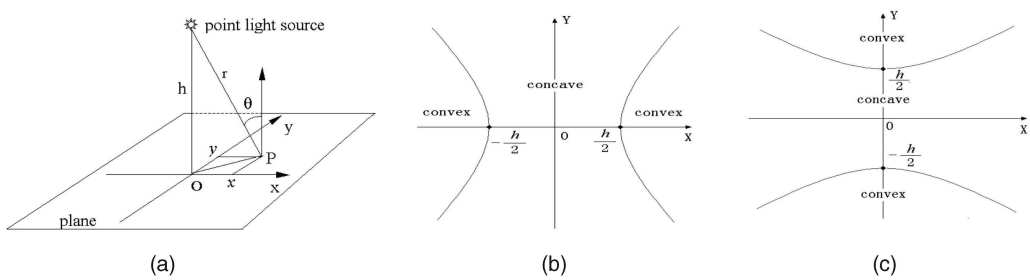

Fig. 2. (a) A point light source. (b) The CID of the point light source on a plane with respect to x. (c) The CID with respect to y.

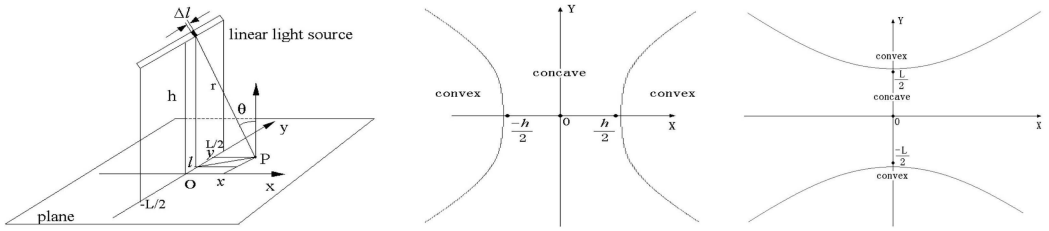

Fig. 3. (a) A linear light source. (b) The CID of the linear light source on a plane with respect to x. (c) The CID with respect to y.

source on the plane and P is a point on the plane. Our motivation is to calculate the illumination at P first and then study its convexity with respect to the x or y direction.

Assume that the luminous intensity of the point light source is I, the distance between the light source and the plane is h, the distance from the light source to P is r, and the incident angle of the light from the light source to P is θ. According to the Square and Cosine law of light [19], the illumination at point P is

$$Ip(x,y) = I\frac{\cos\theta}{r^2} = \frac{Ih}{\sqrt{(x^2+y^2+h^2)^3}}. \tag{1}$$

Next, we will calculate the CID with respect to the x and y directions, respectively.

2.1.1 CID with Respect to x

First, we examine the illumination distribution feature with respect to x. The convexity of a function can be calculated by means of the second derivative. Let $\partial^2 Ip(x,y)/\partial x^2 = 0$. Then, we have

$$\frac{1}{\sqrt{(x^2+y^2+h^2)^5}} - \frac{5x^2}{\sqrt{(x^2+y^2+h^2)^7}} = 0. \tag{2}$$

The solutions to (2) are $x = \pm\sqrt{y^2+h^2}/2$.

Thus, as illustrated in Fig. 2b, when $-\sqrt{y^2+h^2}/2 < x < \sqrt{y^2+h^2}/2$, $Ip(x,y)$ is concave with respect to x. Moreover, when $x < -\sqrt{y^2+h^2}/2$ or $x > \sqrt{y^2+h^2}/2$, $Ip(x,y)$ is convex with respect to x.

Notice that the above solutions have no relationship to the intensity of the light source. This is important because it means that once the light apparatus is made, its CID is established no matter how the intensity of the light sources changes.

2.1.2 CID with Respect to y

For a point light source, we can simply use the symmetry to obtain the CID with respect to y. Let $\partial^2 Ip(x,y)/\partial y^2 = 0$. Then, we obtain

$$\frac{-3Ih}{\sqrt{(x^2+y^2+h^2)^5}} + \frac{15Ihy^2}{\sqrt{(x^2+y^2+h^2)^7}} = 0. \tag{3}$$

The solutions to (3) are $y = \pm\sqrt{x^2+h^2}/2$ and the convexity of $Ip(x,y)$ with respect to y is shown in Fig. 2c.

2.2 CID of a Linear Light Source

A linear light source is another popular light model.

In Fig. 3a, there is a linear light source above the plane. Its length is L, its luminous intensity is I, and the distance to the plan is h. By taking Δl of L as a point light source, we can derive the illumination at P produced by

$$\Delta Ip(x,y) = \frac{Ih\Delta l}{\sqrt{(x^2+y^2+h^2)^3}}. \tag{4}$$

Thus, the whole illumination of the linear light source at P is [20]

$$\begin{aligned} Ip(x,y) &= \int_{-L/2}^{L/2} \frac{Ih}{\sqrt{(x^2+(l-y)^2+h^2)^3}}dl \\ &= \frac{Ih(L/2-y)}{(x^2+h^2)\sqrt{(L/2-y)^2+x^2+h^2}} \\ &\quad + \frac{Ih(L/2+y)}{(x^2+h^2)\sqrt{(L/2+y)^2+x^2+h^2}}. \end{aligned} \tag{5}$$

2.2.1 CID with Respect to x

In a similar fashion as in point light source, let $\partial^2 Ip(x,y)/\partial x^2 = 0$. Then, we can determine the convex and concave areas with respect to x on the plane:

$$\begin{aligned} 0 &= (6x^2-2h^2) \\ &\left(\frac{L/2-y}{\sqrt{(L/2-y)^2+x^2+h^2}} + \frac{L/2+y}{\sqrt{(L/2+y)^2+x^2+h^2}}\right) \\ &+ (3x^2-h^2)(x^2+h^2)\left(\frac{L/2-y}{\sqrt{((L/2-y)^2+x^2+h^2)^3}}\right. \\ &\left. + \frac{L/2+y}{\sqrt{((L/2+y)^2+x^2+h^2)^3}}\right) + 3x^2((x^2+h^2)^2) \\ &\left(\frac{L/2-y}{\sqrt{((L/2-y)^2+x^2+h^2)^5}} + \frac{L/2+y}{\sqrt{((L/2+y)^2+x^2+h^2)^5}}\right). \end{aligned} \tag{6}$$

Equation (6) is too complicated to find direct solutions, so we use a numerical analysis to solve the problem. Fig. 3b

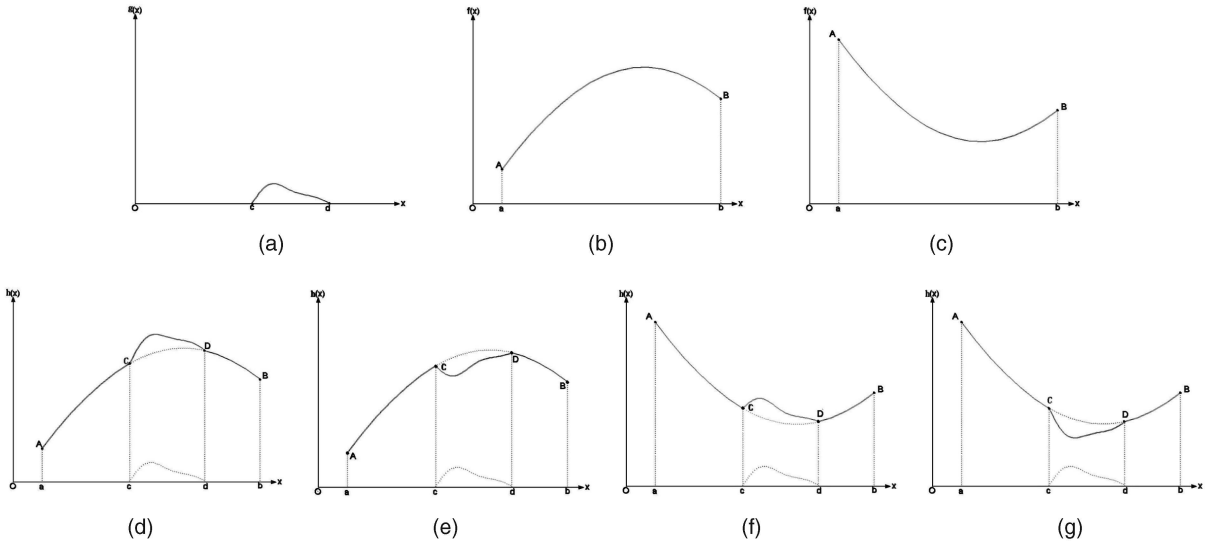

Fig. 4. Relationship between the object and its background. (a) Object signal. (b) Concave background. (c) Convex background. (d) Concave background with brighter objects. (e) Concave background with darker objects. (f) Convex background with brighter objects. (g) Convex background with darker objects.

illustrates the solutions to (6), from which we find that the plane is divided into three parts: The central part is a strict concave area and the far two sides are strict convex areas.

2.2.2 CID with Respect to y

Symmetry is no longer applicable for linear light sources. Therefore, we have to derive the second partial derivative of $Ip(x, y)$ with respect to y first and then let $\partial^2 Ip(x, y)/\partial y^2 = 0$. Finally, we obtain the equation determining the convexity:

$$\frac{y + L/2}{\sqrt{\left((L/2 + y)^2 + x^2 + h^2\right)^5}} = \frac{y - L/2}{\sqrt{\left((y - L/2)^2 + x^2 + h^2\right)^5}}. \tag{7}$$

The solutions to (7) are

$$x^2 = \frac{\sqrt[5]{(y-L/2)^2}((y+L/2)^2+h^2) - \sqrt[5]{(y+L/2)^2}((y-L/2)^2+h^2)}{\sqrt[5]{(y+L/2)^2} - \sqrt[5]{(y-L/2)^2}}. \tag{8}$$

We plot the solutions to (8) in Fig. 3c, from which we observe that the plane is also divided into three parts: the central part and the two side parts. For a fixed x, the central part is a concave area where $\partial^2 Ip(x, y)/\partial y^2 < 0$ with respect to y and the two side parts are convex areas where $\partial^2 Ip(x, y)/\partial y^2 > 0$ with respect to y. It is obvious that the central part is more useful because the illumination becomes weak in the two side areas.

If an illumination profile $Ip(x, y)$ is available, we can attempt to sample known background points and reconstruct the background. Thereby, after analyzing the CID of those light sources, we then will find out how to put it into use to reconstruct the image background for images having objects with unclear edges against the nonuniform background.

3 Proposed Segmentation Algorithm

3.1 Methodology

Suppose that $g(x)$, as shown in Fig. 4a, is the object signal, $f_\cap(x)$ is the concave background, and $f_\cup(x)$ is convex, shown in Figs. 4b and 4c, respectively. As mentioned at the beginning of Section 1, we only deal with images having darker objects against a brighter background or vice versa. Therefore, the relationship between the object and the background can be simply divided into the following four cases:

1. a concave background with brighter objects (see Fig. 4d), where $h(x) = f_\cap(x) + g(x)$,
2. a concave background with darker objects (see Fig. 4e), where $h(x) = f_\cap(x) - g(x)$,
3. a convex background with brighter objects (see Fig. 4f), where $h(x) = f_\cup(x) + g(x)$, and
4. a convex background with darker objects (see Fig. 4g), where $h(x) = f_\cup(x) - g(x)$.

According to the properties of convex and concave functions, if $f(x)$ is a convex function, then $-f(x)$ becomes a concave one and vice versa. Thereby, the above four cases can be reduced to only two:

1. a convex background with darker objects or a concave background with brighter objects and
2. a convex background with brighter objects or a concave background with darker objects.

As a result, we will only discuss two cases, namely, a concave background with darker objects and a convex background with darker objects; the other two cases can be processed in the same way by inversing.

However, how can we reconstruct the background by means of the CID? Our strategy is to use the CID and the relationship between the background and objects to find some points belonging to the background first and then use some of those points to reconstruct the whole background. Hence, the segmentation framework is presented in Fig. 5.

Usually, the first step of an image processing method is noise removal. Two noise models can adequately represent most noises added to images: additive Gaussian noise and impulse noise [23]. Those noises have no relationship to the

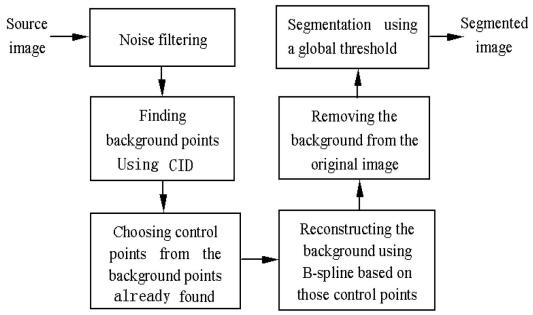

Fig. 5. Flowchart of the proposed algorithm.

CID; we can just employ the Weiner filter or other low-pass filters to reduce them. Here, we will not discuss more; we will focus on how to find the background points and use them to reconstruct the background.

3.2 Finding Background Points from the Concave Background

In a digital image, signals are stored in a discrete form. As a part of a digital image, the concave background is also digitized into a discrete form; an example appears in Fig. 6a, which is a scan line of an image. After digitizing, the concave background becomes a set of points that build up a convex hull. Thereby, we could use a convex hull algorithm to find those points belonging to the background.

Finding the convex hull of a set of points is the most elementary and interesting problem in computational geometry. Its main purpose is to find the smallest convex polygon containing all the points of a set. The Graham scan algorithm [22] is the most popular one among so many convex hull-building algorithms. Although the Graham algorithm does not generalize to three dimensions (3D) and higher dimensions, it has a low runtime constant in two dimensions (2D). For a digital image, all of the pixels of one scan line compose a set of points S in 2D. According to the definition of the concave function, if there is no object signal, like in Fig. 6a, all of the samples of the concave background would build up a convex hull and the line segment between the two endpoints PQ is the underside part of the convex hull. However, when a signal is embedded on the background, like in Fig. 6b, some points S_1 of the background would be pulled down from the convex hull, whereas other points S_2, where $S = S_1 \cup S_2$, would still be in the original positions. If we use the convex hull algorithm again to find the new convex hull, these points S_2 will remain to build up the new

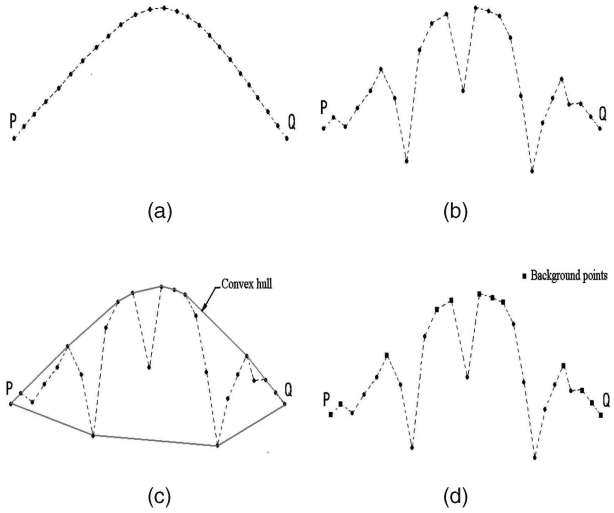

Fig. 6. (a) A discrete concave background. (b) Background with signal. (c) Convex hull of (b). (d) Background points found.

convex hull, as shown in Fig. 6c. Obviously, PQ divides the new convex hull into upper and lower parts. The upper part contains the background points we are looking for, as shown in Fig. 6d, whereas the lower part would not be taken into account anymore.

3.3 Finding Background Points from the Convex Background

In this case, the object is darker than the background, namely, $h(x) = f_{\cup}(x) - g(x)$, so, according to the definition of a convex function, we have

$$f_{\cup}(\lambda x_1 + (1-\lambda)x_2) - g(\lambda x_1 + (1-\lambda)x_2) \leq \lambda f_{\cup}(x_1) + (1-\lambda) f_{\cup}(x_2), \quad (9)$$

where x_1 and x_2 are two points on the definition domain and $0 < \lambda < 1$. This means that the object between x_1 and x_2 is below the chord composed of $(x_1, h(x_1))$ and $(x_2, h(x_2))$. Therefore, we can use this property to find the points belonging to the background. First, we draw a chord from the left endpoint A to one point X on the scan line to see if other points between A and X are below the chord AX. If it is true, we then take point X as a left candidate for the background point. Fig. 7a illustrates the procedure in which line segments AC, AP, AD, and AB are the chord samples and all of the small squares stand for the left candidate points found. Correspondingly, we draw a chord from the

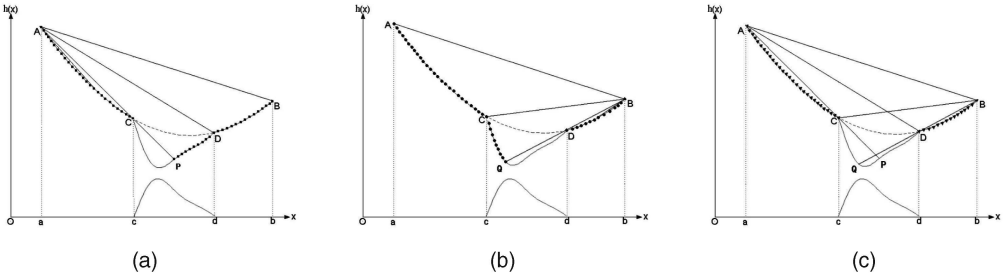

Fig. 7. Finding background points using the convex feature. (a) Finding left background point candidates. (b) Finding right background point candidates. (c) The final background points.

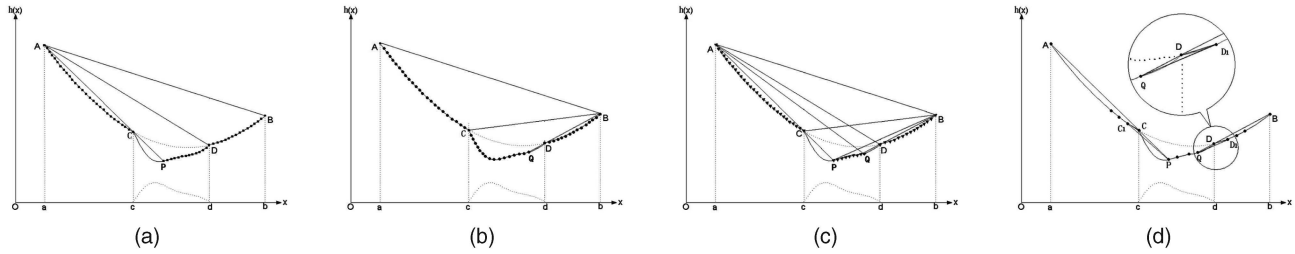

Fig. 8. A special case. (a) Finding left background point candidates. (b) Finding right background point candidates. (c) Background points found with errors. (d) Correcting method.

right endpoint B to one point X to see if other points between B and X are below the chord BX. If they are, we then take point X as a right candidate point for the background. Fig. 7b illustrates how to find such candidates, where line segments BD, BQ, BC, and BA are the chords and all of the small circles are the right candidate points. As the left candidate points and right candidate points are all found according to the method mentioned above, we then select those that belong to both the left and right candidate points to be the background points, as shown in Fig. 7c, in which all of the small triangles are the background points we have found.

Unfortunately, the background points found by the above method are not always true. In Fig. 8a, we see that when we draw a chord from left endpoint A to find the left candidate points of the background, point C is the inflection point, and the points between C and P are taken as the object, but the points between P and D are still taken as the left candidate points of the background which need to be kicked out by the chord from the right endpoint. The same is true for the points between C and Q in Fig. 8b. Thus, the restricted condition is that the points between P and D and the points between C and Q should not share common points, that is, $x_Q < x_P$. However, if $x_Q \geq x_P$, as shown in Fig. 8, the points between P and Q are mistaken as the background points, which leads to the improper segmentation. That case often happens when the object is relatively big compared with the background and has little difference from the background in intensity. We have to find a way to solve this kind of problem.

Before we find the solution to the problem, let us review a property of the convex function. The property is that if $f(x)$ is a convex function on $[a,\ b]$ and $a < x_1 < x_2 < x_3 < b$, then

$$\frac{f(x_2) - f(x_1)}{x_2 - x_1} \leq \frac{f(x_3) - f(x_1)}{x_3 - x_1} \leq \frac{f(x_3) - f(x_2)}{x_3 - x_2}. \qquad (10)$$

This property shows the slope relationship of chords [21], just as shown in Fig. 9.

Therefore, we use this property to solve the problem. In order to make the illustration easier to follow, we redraw Fig. 8c in a simplified form as Fig. 8d. The property tells us that, in Fig. 8d, the slope of line segment C_1P should be greater than that of C_1C but less than that of CP. However, the fact is that the slope of line segment C_1P is neither greater than that of C_1C nor less than that of CP. Therefore, point P should not be taken as the background point. The same step can be applied to point Q and the points between P and Q, as illustrated in Fig. 8d. With the help of this approach, we can rule out those exceptional points. Of course, the adjacent scan lines will also be helpful to kick out those points.

Although we have used the Weiner filter as the first step to suppress the noises, large noises at the endpoints of a scan line may still exist and bring errors to the process. If the noise is darker than the background at the endpoints, as in Fig. 10a, there would be no or only one common background point found by the chords except for the two endpoints. If this case happens, we can simply discard the background points found on this scan line. If the noise is brighter than the background, as in Fig. 10b, it would not affect the background point detection because the corrupted background is still convex.

3.4 Reconstructing the Background

After locating those background points, the next step is to reconstruct the background. Piecewise bidimensional polynomial functions are frequently used in this situation. Since errors exist in the background points that we found, an approximate representation is a better choice. Therefore, we use a spline function to make the approximation. Among all kinds of spline, B-spline is the one that has been most widely used for its special properties, such as continuity, smoothness, etc. Therefore, we will use the B-spline to reconstruct the background.

3.4.1 Selecting Control Points

In the above section, we learned that, in order to reconstruct the background using B-spline, control points have to be appointed first. It is true that we have found numerous background points, but there is no need to take all of them as the control points. The criterion to select control points is that those points should distribute on the background as uniformly as possible. According to this rule, we can simply appoint control points with uniform intervals of coordinates so that the selected points would distribute on the background uniformly. However, most of the time, the appointed pixels with uniform intervals are not the background points we have found. If that occurs, we have to

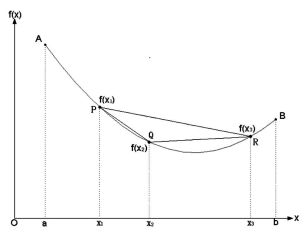

Fig. 9. Geometric relationship between three chords of a convex function.

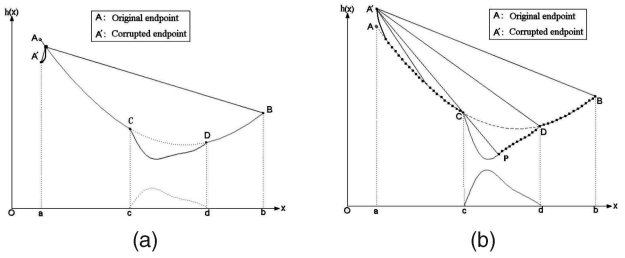

Fig. 10. Cases with endpoints corrupted by large noises. (a) Corrupted by noise darker than the background. (b) Corrupted by noise brighter than the background.

search around the pixel to find the nearest background point to replace it.

3.4.2 Reconstructing the Background Using B-Spline

The definition of B-Spline is complicated; Unser [24] summarized it well. We will employ the most commonly used cubic, that is, periodic B-spline, to reconstruct the background. A piece of cubic B-spline is represented by four points as follows:

$$Q(t) = TMP, \quad 0 \le t \le 1, \tag{11}$$

where $T = \begin{bmatrix} t^3 & t^2 & t^1 & 1 \end{bmatrix}$,

$$M = \frac{1}{6}\begin{bmatrix} -1 & 3 & -3 & 1 \\ 3 & -6 & 3 & 0 \\ -3 & 0 & 3 & 0 \\ 1 & 4 & 1 & 0 \end{bmatrix},$$

and $P = [P_i \quad P_{i+1} \quad P_{i+2} \quad P_{i+3}]^T$ are the four control points.

Fig. 11 shows two consecutive pieces of B-spline, from which we can see that 1) B-spline does not pass through any of the control points and 2) B-spline is smoother than the line segments connected by the control points and acts like a low-pass filter.

With the expression of the cubic B-spline known, it is easy to construct a bicubic B-spline:

$$Q(u, v) = U \cdot M \cdot P \cdot M^T \cdot V^T, \tag{12}$$

where $U = \begin{bmatrix} u^3 & u^2 & u^1 & 1 \end{bmatrix}$, $V = \begin{bmatrix} v^3 & v^2 & v^1 & 1 \end{bmatrix}$, $0 \le u, v \le 1$,

$$P = \begin{bmatrix} p_{11} & p_{12} & p_{13} & p_{14} \\ p_{21} & p_{22} & p_{23} & p_{24} \\ p_{31} & p_{32} & p_{33} & p_{34} \\ p_{41} & p_{42} & p_{43} & p_{44} \end{bmatrix}$$

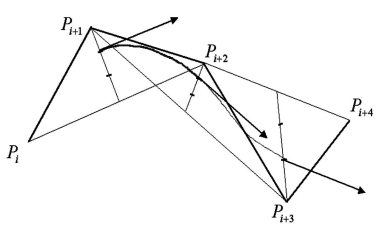

Fig. 11. Two consecutive pieces of a cubic B-spline curve.

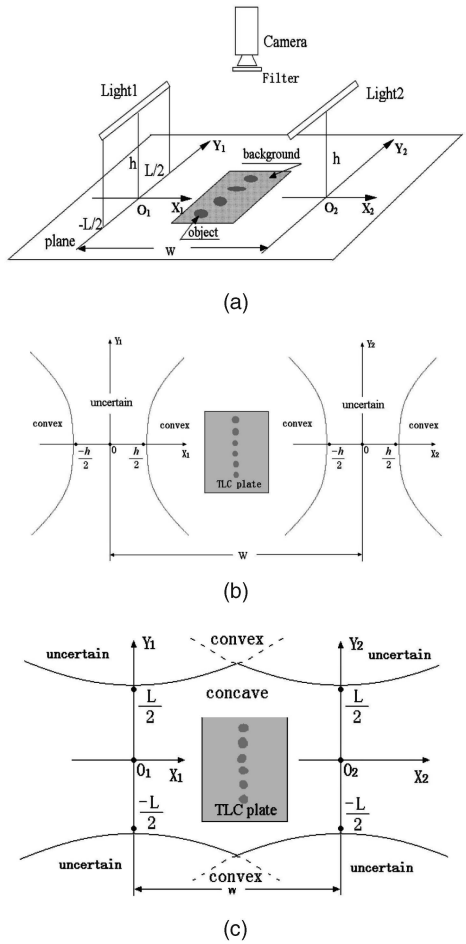

Fig. 12. (a) The linear light source apparatus of the experiment. (b) The rough CID with respect to x. (c) The rough CID with respect to y.

is the matrix of 16 control points in neighborhood and M is just the same as that in (11).

4 Experiment Results

In this section, we will evaluate the proposed method by segmenting the images obtained in TLC, a widely used chemical analysis method.

4.1 Experimental Instrumentation

In TLC, a plate coated with special materials that can absorb ultraviolet to emit fluorescence is used as the TLC plate. The chemical substances that need to be measured are sampled onto the plate and are developed. Usually, the substances do not emit fluorescence. Therefore, by measuring the intensity difference between the substances and the background, we can make the quantitative evaluation.

In our experiment, the developed TLC plate containing chemical substances is placed under two parallel linear ultraviolet light sources, Light1 and Light2, as shown in Fig. 12a. The two light sources are both 10 cm high above the TLC plate. Their wavelength is 254 nm and their geometric length is $L = 14$ cm. The distance between the two light sources is $W = 27$ cm. A digital camera is mounted above the cabinet for capturing images of the TLC plate. The horizontal direction of the image captured by the camera is parallel to the x axis.

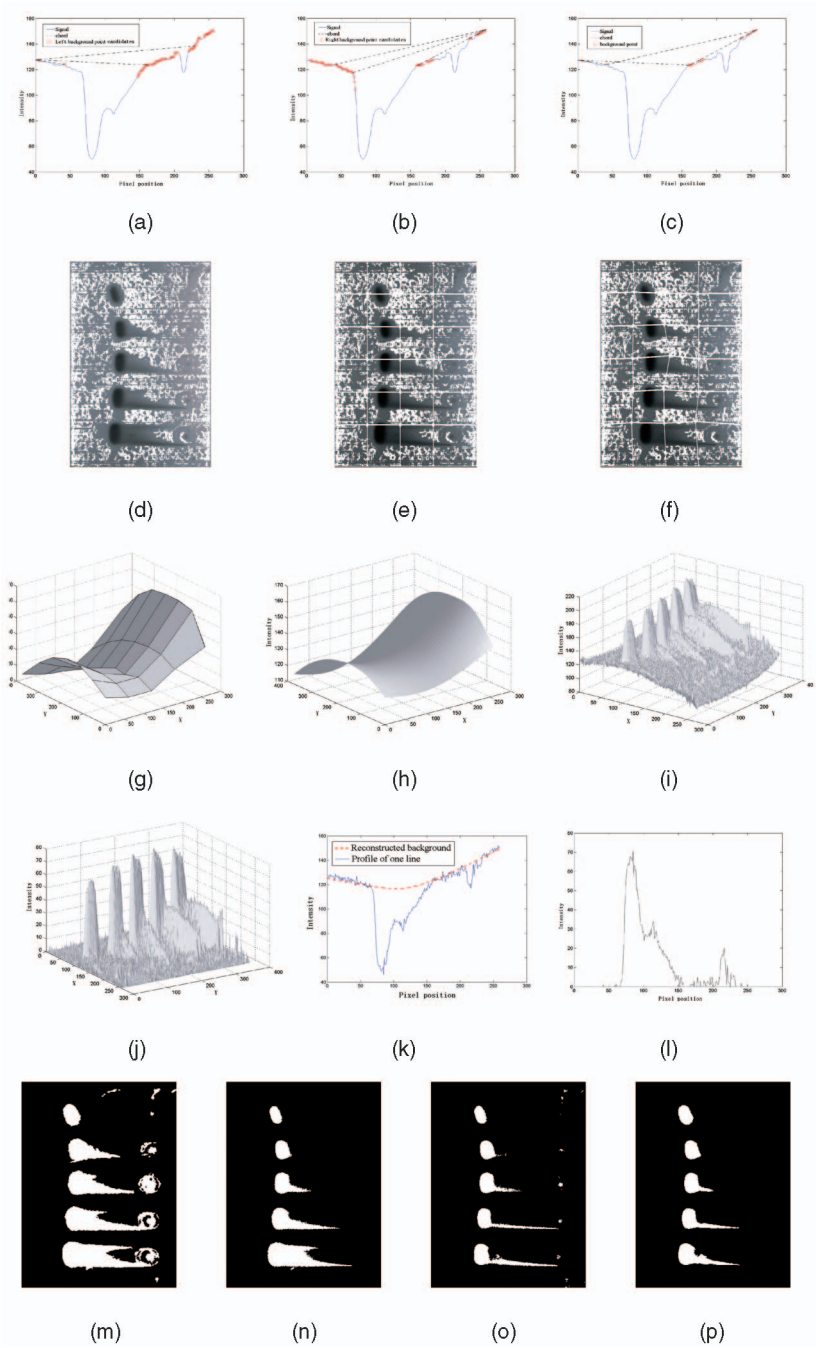

Fig. 13. (a), (b), and (c) Finding background points of a scan line using a chord algorithm. (d) All of the background points found (bright pixels). (e) Control points appointed in uniform intervals. (f) Control points modified. (g) The 3D plot of the grid in (f). (h) The background reconstructed by B-spline. (i) The 3D plot of Fig. 1a (reversed). (j) Output of (i) subtracting (h). (k) A scan line with the background reconstructed. (l) The scan line with the background removed. (m) Final segmentation of Fig. 1a. (n) Otsu's segmentation. (o) Yanowitz and Bruckstein's segmentation. (p) Kim et al.'s segmentation.

With reference to Fig. 3b, we can conclude that if the two parallel linear light sources in Fig. 12a are far enough apart, there is an area between them in which the CID with respect to x is convex because the additive property of a convex function tells us that the sum of two convex functions is still convex; Fig. 12b shows the convexity. Similarly, we can obtain the concave distribution with respect to y, as shown in Fig. 12c. It should be pointed out that it does not matter whether the intensities of the two linear light sources are identical or not since the CID has no relationship to the intensity, as we point out in Section 2.

Fig. 1a is such an image captured by the camera in Fig. 12a. Since the horizontal direction of the image is parallel to the x axis in Fig. 12a and the intensity of the image is proportional to the illumination [25], the background of the image is convex with respect to the horizontal direction and concave with respect to the vertical direction.

4.2 Segmentation Based on the Convex Feature

Because the background in Fig. 1a is convex with respect to the horizontal direction, we take a scan line of it as the

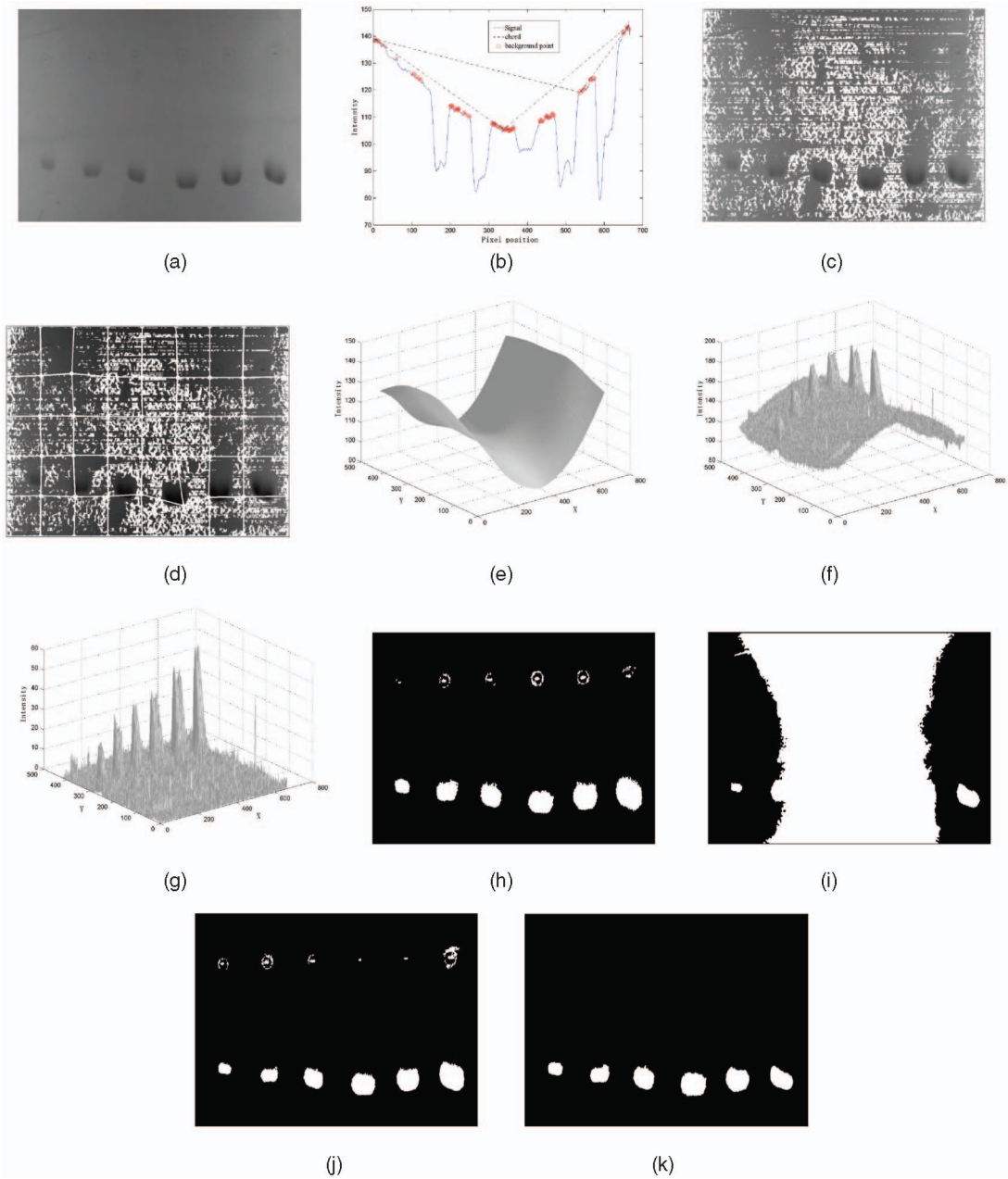

Fig. 14. (a) Original image of experiment 2. (b) The profile of a scan line and the background points found by a chord algorithm. (c) All of the background points found (bright pixels). (d) Control points selected. (e) The background reconstructed by B-spline. (f) The 3D plot of (a) (reversed). (g) Output of (f) subtracting (e). (h) Final segmentation result. (i) Otsu's segmentation. (j) Yanowitz and Bruckstein's segmentation. (k) Kim et al.'s segmentation.

example to show the process of searching for background points using the convex feature. First, we draw chords from the left endpoint to another point to test if it is a possible background point according to the approach mentioned in Section 3.3. If it is true, then we mark it as a left background point candidate. The square marks in Fig. 13a are the left background point candidates found by left chords. The right background point candidates can be found in the same way; they are the triangular marks in Fig. 13b. Next, we choose points belonging to both the left and right background point candidates to be the final background points of the line. The circle marks in Fig. 13c are the final background points we expect. After every line in Fig. 1a is processed, we obtain the background points belonging to the whole image. The white pixels in Fig. 13d are the background points we have found. Next, we try to choose the control points. The grid in Fig. 13e is built up by the control points appointed in uniform coordinate intervals where some appointed control points are not background points and Fig. 13f shows the modified grid in which all of the control points are from background points. Fig. 13g illustrates the 3D plot of the grid in Fig. 13f and Fig. 13h is the background reconstructed by B-spline. Now that the background has been found, it is easy to remove the background from the original image. Fig. 13i is the 3D plot of Fig. 1a and Fig. 13j is the corresponding 3D plot with the background removed. In order to see more clearly, we show Fig. 1c and its reconstructed background in profile

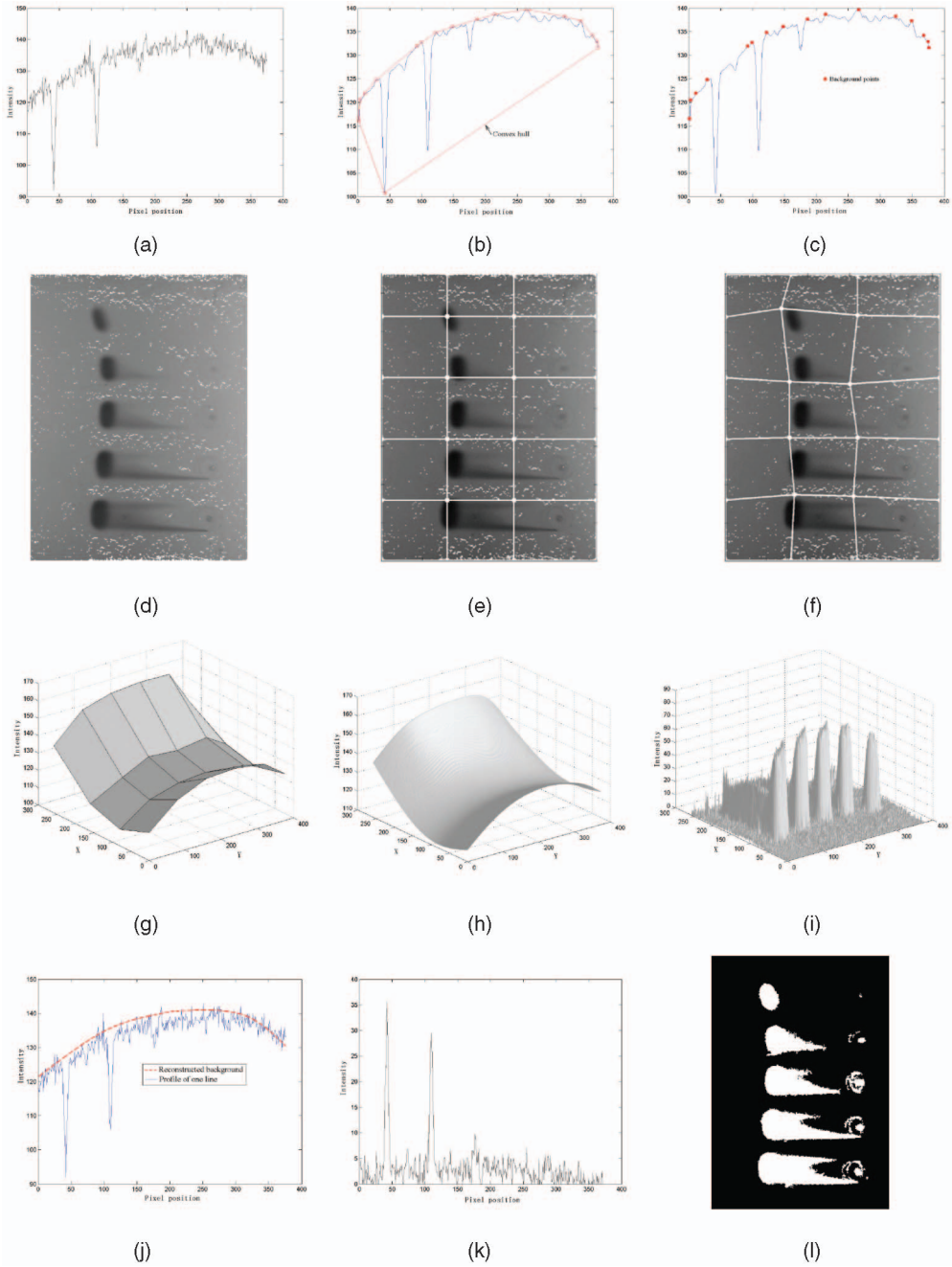

Fig. 15. (a) Profile of one column in Fig. 1a. (b) Finding the convex hull of (a) after noise filtering. (c) Background points found for (a). (d) All of the background points found for Fig. 1a (the bright pixels). (e) Control points appointed in uniform intervals. (f) Control points modified. (g) The 3D plot of the grid in (f). (h) The background reconstructed by B-spline. (i) Output with the background removed. (j) The column with its background reconstructed. (k) The column with the background removed. (l) Final segmentation.

forms in Fig. 13k and the corresponding output with the background removed is presented in Fig. 13l. Fig. 13m gives the final segmentation output with a global threshold applied to Fig. 13j and noises removed.

We also use other various methods mentioned in Section 1 to make the segmentation for comparison. They are Otsu's segmentation, a global threshold method; Yanowitz and Bruckstein's segmentation, a background surface reconstruction method; and Kim et al.'s segmentation, a water flow model method. Each of those segmentation outputs are illustrated as Figs. 13n, 13o, and 13p, respectively.

In order to test the robustness of the method, another experiment is made. This time, all of the samples are arranged horizontally so that there would be a scan line that can pass through several samples. The corresponding processing results are illustrated in Fig. 14, where the noises of the segmentation results are removed.

4.3 Segmentation Based on the Concave Feature

In this section, we will use the concave feature to make the segmentation of Fig. 1a. Since the background in Fig. 1a is concave with respect to the vertical direction, we will take a column of it as an example to show the procedure.

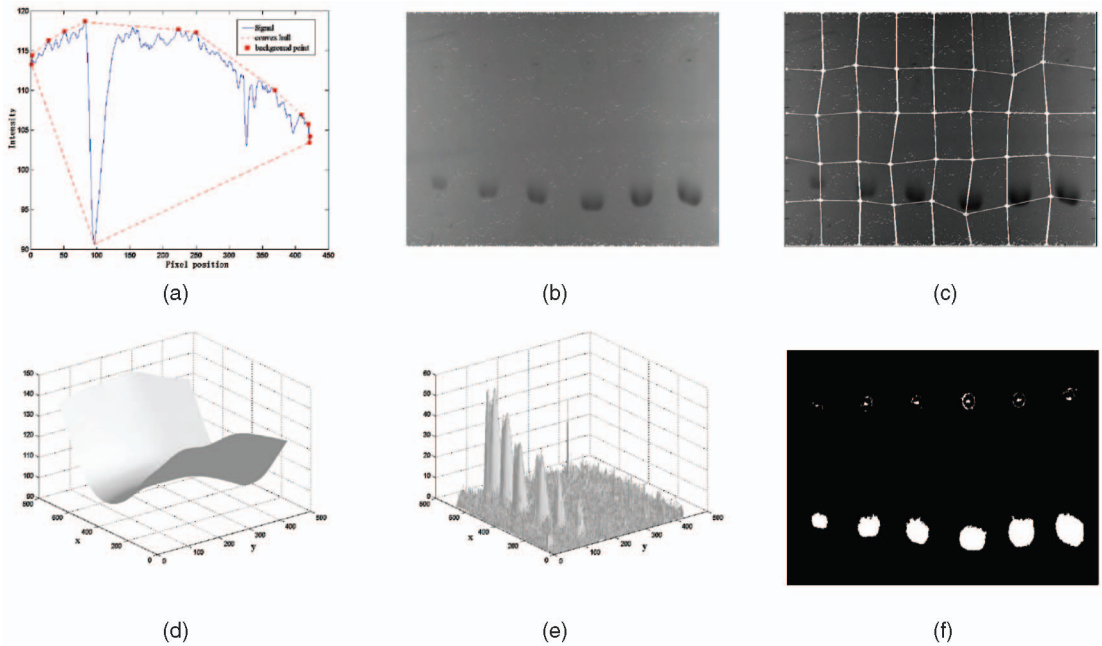

Fig. 16. (a) Profile of one column in Fig. 14a and the corresponding background points found by the convex hull method. (b) All of the background points found for Fig. 14a (the bright pixels). (c) Control points selected. (d) The background reconstructed by B-spline. (e) Output with the background removed. (f) Final segmentation result.

The processing steps for the second experiment using the concave feature are illustrated in Fig. 16.

Fig. 15a shows the profile of a column in Fig. 1a. When the convex hull of that column is found, the points on the upside part of the convex hull are taken as the background points, as shown in Figs. 15b and 15c. Fig. 15d illustrates all of the background points found for the whole image. Figs. 15e and 15f show how to select control points. Fig. 15h shows the reconstructed background based on B-spline. Fig. 15l is the final result of the segmentation.

4.4 Quantitative Evaluation

After separating the objects from the background, we will make a quantitative evaluation to test the performance of the proposed method. We will take experiment 1 as an example to make the quantitative analysis in detail. In Fig. 1a, there are five samples or objects that are from the same compound; their concentrations are prepared in linearity in the experiment. When those samples are developed from right to left on their lanes, the residues make their edges unclear. It is said that the sample's intensity integration is proportional to its concentration [26]. Therefore, if the concentrations of the samples are prepared in linearity, their intensity integrations are expected to be linear too. Thus, our purpose is to test if the intensity integrations of those samples are linear based on the proposed segmentation results.

According to the samples' lanes, we divide the original image into five blocks manually, $D_1, D_2, \cdots, D_5$, as shown in Fig. 17a. Assume that $g(x,y)$ and $d(x,y)$ stand for the intensity of the pixel at location (x,y) in Figs. 13j and 13m, respectively; we calculate the intensity integration for each sample by

$$f_i = \sum_{d(x,y)\in D_i} g(x,y)d(x,y), \quad i = 1,2,\ldots,5. \tag{13}$$

Notice that $d(x,y)$ has only two values, 0 or 1, as Fig. 13m shows.

Then, we use the following formula to calculate the linear correlation coefficient R between the samples' intensity integrations and their concentrations:

$$R = \frac{1}{n-1}\sum_{i=1}^{n}\left(\frac{f_i - \bar{f}}{S_f}\right)\left(\frac{c_i - \bar{c}}{S_c}\right), \tag{14}$$

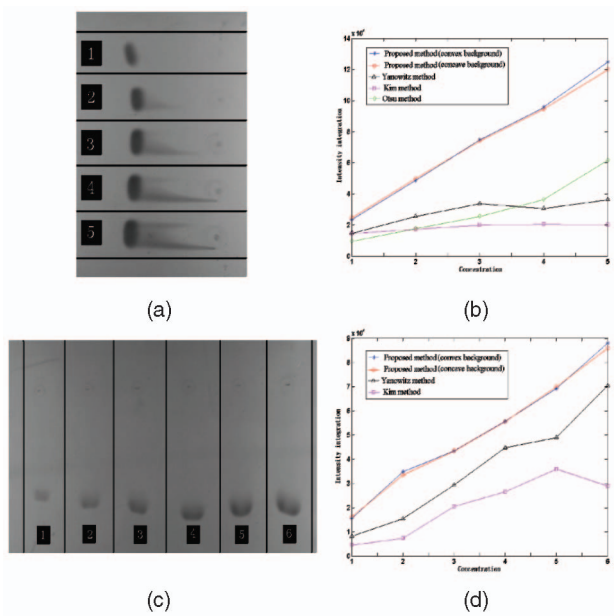

Fig. 17. (a) Sample blocks of experiment 1. (b) Relationship between the sample concentrations and their intensity integrations in experiment 1. (c) Sample blocks of experiment 2. (d) Relationship between the sample concentrations and their intensity integrations in experiment 2.

TABLE 1
Experiment 1: Linear Correlation Coefficients Obtained by Different Methods

Method	Convex	Concave	Yanowitz	Kim	Otsu
R	0.9991	0.9995	0.8959	0.8872	0.9623

TABLE 2
Experiment 2: Linear Correlation Coefficients Obtained by Different Methods

Method	Convex	Concave	Yanowitz	Kim
R	0.9942	0.9974	0.9882	0.9178

where n is the number of samples (here, it is 5), f_i and c_i are the intensity integration and the concentration of sample i, respectively, $\bar{f}$ and $\bar{c}$ are the average values of f and c, respectively, and S_f and S_c are the standard deviations of f and c, respectively. If R is much closer to 1, then we say that the segmentation is better. For experiment 1, R is 0.9991 when the segmentation based on the convex feature is used and it becomes 0.9995 when the segmentation result based on the concave feature is employed. Compared with 0.9955, the coefficient R given by Chau et al. [27], who used a flatbed scanner to scan the TLC plate and found the background manually, the proposed method's results are on the same level or even better. For comparison, the other segmentation results presented in Fig. 13 are made quantitative evaluations too. Those evaluation data is listed in Table 1 and Fig. 17b shows them visually.

With the same quantitative evaluation method mentioned above used, the corresponding evaluation data obtained for the second experiment are listed in Table 2 and Fig. 17d illustrates those data visually. Since Otsu's method does not work in this experiment, there is no evaluation data about this method given in Table 2.

From the above experiments, we can see that both the convex background and the concave background method can work well no matter how blurry the edge of the samples becomes. However, the segmentation output given by Yanowitz and Bruckstein's method would become worse if the edge becomes blurrier because it is an edge-sensitive method. If the background becomes more uneven, Otsu's method would not work as it is a global threshold method. Kim et al.'s method uses water flow to make the segmentation; if the objects are on a nonuniform background, it could separate them from the background but not completely.

It should be pointed out that, because the nonuniform illumination also affects the intensity of the samples, calibration should be taken into account during practical chemical analysis [28]. If so, the linear correlation coefficients obtained by the proposed methods would become better.

5 Conclusions

Light plays an important role in computer vision; knowing more about its features would make the applications easier and robust. This paper presents such an example which uses the illumination distribution features of the light sources.

To separate objects with unclear edges from the nonuniform background, traditional methods usually consider the gray-level relationship between objects and their background only, so the segmentation outputs are not so satisfying sometimes. This paper presents a novel method that uses the CID of the light sources to find pixels belonging to the background first and then reconstructs the background using B-spline based on the control points selected from the background points found. With the removal of the background from the original image, it is easy to obtain the precise segmentation. Although the paper uses the CID of light sources, it does not have a relationship to the intensity of the light source, which is a variable factor in a light apparatus. From the evaluation experiments, it can be seen that the proposed method could separate objects with unclear edges accurately from the nonuniform background. The trade-off is that we have to know the CID of the light sources first and make the segmentation in situ.

Appendix A

A.1 Second Partial Derivatives of the Illumination of the Point Light Source

According to the theorems determining the convexity of a function by means of the second derivative, we derive the second partial derivative of $Ip(x, y)$ of (1) with respect to x here.

Since

$$\frac{\partial Ip(x,y)}{\partial x} = \frac{-3xIh}{\sqrt{(x^2+y^2+h^2)^5}}, \tag{15}$$

we have

$$\frac{\partial^2 Ip(x,y)}{\partial x^2} = \frac{-3Ih}{\sqrt{(x^2+y^2+h^2)^5}} + \frac{15Ihx^2}{\sqrt{(x^2+y^2+h^2)^7}}. \tag{16}$$

According to the symmetry, we can easily obtain

$$\frac{\partial^2 Ip(x,y)}{\partial y^2} = \frac{-3Ih}{\sqrt{(x^2+y^2+h^2)^5}} + \frac{15Ihy^2}{\sqrt{(x^2+y^2+h^2)^7}}. \tag{17}$$

A.2 Second Partial Derivatives of the Illumination of the Linear Light Source

Similarly, we derive the second partial derivative of $Ip(x, y)$ of (5) with respect to x.

Since

$$\frac{\partial Ip(x,y)}{\partial x} = \frac{-2Ihx}{(x^2+h^2)^2}\left(\frac{L/2-y}{\sqrt{(L/2-y)^2+x^2+h^2}}+\frac{L/2+y}{\sqrt{(L/2+y)^2+x^2+h^2}}\right)+\frac{Ih}{x^2+h^2}\left(\frac{-x(L/2-y)}{\sqrt{((L/2-y)^2+x^2+h^2)^3}}+\frac{-x(L/2+y)}{\sqrt{((L/2+y)^2+x^2+h^2)^3}}\right), \tag{18}$$

we have

$$\frac{\partial^2 Ip(x,y)}{\partial x^2} = \frac{-2Ih}{(x^2+h^2)^2}\left(\frac{L/2-y}{\sqrt{(L/2-y)^2+x^2+h^2}}+\frac{L/2+y}{\sqrt{(L/2+y)^2+x^2+h^2}}\right)+\frac{8Ihx^2}{(x^2+h^2)^3}\left(\frac{L/2-y}{\sqrt{(L/2-y)^2+x^2+h^2}}+\frac{L/2+y}{\sqrt{(L/2+y)^2+x^2+h^2}}\right)+\frac{-2Ihx}{(x^2+h^2)^2}\left(\frac{-x(L/2-y)}{\sqrt{((L/2-y)^2+x^2+h^2)^3}}+\frac{-x(L/2+y)}{\sqrt{((L/2+y)^2+x^2+h^2)^3}}\right)+\frac{-Ih}{x^2+h^2}\left(\frac{L/2-y}{\sqrt{((L/2-y)^2+x^2+h^2)^3}}+\frac{L/2+y}{\sqrt{((L/2+y)^2+x^2+h^2)^3}}\right)+\frac{2Ihx^2}{(x^2+h^2)^2}\left(\frac{L/2-y}{\sqrt{((L/2-y)^2+x^2+h^2)^3}}+\frac{L/2+y}{\sqrt{((L/2+y)^2+x^2+h^2)^3}}\right)+\frac{-Ihx}{x^2+h^2}\left(\frac{-3x(L/2-y)}{\sqrt{((L/2-y)^2+x^2+h^2)^5}}+\frac{-3x(L/2+y)}{\sqrt{((L/2+y)^2+x^2+h^2)^5}}\right). \tag{19}$$

For the linear light source, the symmetry is no longer useful. We have to derive the second partial derivative of $Ip(x,y)$ of (5) with respect to y.

Since

$$\frac{\partial Ip(x,y)}{\partial y} = \frac{Ih}{\sqrt{((y+L/2y)^2+x^2+h^2)^3}} - \frac{Ih}{\sqrt{((y-L/2)^2+x^2+h^2)^3}}, \tag{20}$$

we have

$$\frac{\partial^2 Ip(x,y)}{\partial y^2} = -\frac{3Ih(L/2+y)}{\sqrt{((L/2+y)^2+x^2+h^2)^5}} + \frac{3Ih(y-L/2)}{\sqrt{((y-L/2)^2+x^2+h^2)^5}}. \tag{21}$$

ACKNOWLEDGMENTS

This work was supported by the Natural Science Foundation of China under Grant 60572087.

REFERENCES

[1] S.D. Yanowitz and A.M. Bruckstein, "A New Method for Image Segmentation," *Computer Vision, Graphics, and Image Processing*, vol. 46, no. 1, pp. 82-95, Apr. 1989.
[2] N. Otsu, "A Threshold Selection Method from Gray-Level Histograms," *IEEE Trans. Systems, Man, and Cybernetics*, vol. 9, no. 1, pp. 62-66, Jan. 1979.
[3] O.D. Trier and A.K. Jain, "Goal-Directed Evaluation of Binarization Methods," *IEEE Trans. Pattern Analysis and Machine Intelligence*, vol. 17, no. 12, pp. 1191-1201, Dec. 1995.
[4] C.K. Chow and T. Kaneko, "Boundary Detection of Radiographic Images by a Threshold Method," *Proc. IFIP Congress*, pp. 1530-1535, 1971.
[5] Y. Nakagawa and A. Rosenfeld, "Some Experiments on Variable Thresholding," *Pattern Recognition*, vol. 11, no. 3, pp. 191-204, 1979.
[6] S.M.X. Fernando and D.M. Monro, "Variable Thresholding Applied to Angiography," *Proc. Sixth Int'l Conf. Pattern Recognition*, 1982.
[7] T. Pun, "A New Method for Gray-Level Picture Thresholding Using the Entropy of the Histogram," *Signal Process*, vol. 2, no. 3, pp. 223-237, 1980.
[8] A. Dawound and M.S. Kamel, "Iterative Multimodel Subimage Binarization for Handwritten Character Segmentation," *IEEE Trans. Image Processing*, vol. 13, no. 9, pp. 1223-1330, Sept. 2004.
[9] Q. Huang, W. Gao, and W.J. Cai, "Thresholding Technique with Adaptive Window Selection for Uneven Lighting Image," *Pattern Recognition Letters*, vol. 26, pp. 801-808, 2005.
[10] F.H.Y. Chan, F.K. Lam, and H. Zhu, "Adaptive Thresholding by Variational Method," *IEEE Trans. Image Processing*, vol. 7, no. 3, pp. 468-473, Mar. 1998.
[11] I. Blayvas, A. Bruckstein, and R. Kimmel, "Efficient Computation of Adaptive Threshold Surfaces for Image Binarization," *Pattern Recognition*, vol. 39, no. 1, pp. 89-101, 2006.
[12] F. Liu, X.D. Song, Y.P. Luo, and D.C. Hu, "Adaptive Thresholding Based on Variational Background," *Electronics Letters*, vol. 38, no. 18, pp. 1017-1018, Aug. 2002.
[13] I.K. Kim, D.W. Jung, and R.H. Park, "Document Image Binarization Based on Topographic Analysis Using a Water Flow Model," *Pattern Recognition*, vol. 35, pp. 265-277, 2002.
[14] H.H. Oh, K.T. Lim, and S.I. Chien, "An Improved Binarization Algorithm Based on a Water Flow Model for Document Image with Inhomogeneous Backgrounds," *Pattern Recognition*, vol. 38, pp. 2612-2625, 2005.
[15] T. Wada, H. Ukida, and T. Matsuyama, "Shape from Shading with Interreflections under a Proximal Light Source: Distortion-Free Copying of an Unfolded Book," *Int'l J. Computer Vision*, vol. 24, pp. 125-135, 1997.

[16] C.L. Tan, L. Zhang, Z. Zhang, and T. Xia, "Restoring Warped Document Images through 3D Shape Modeling," *IEEE Trans. Pattern Analysis and Machine Intelligence,* vol. 28, no. 2, pp. 195-208, Feb. 2006.
[17] R. Zhang, P.S. Tsai, J.E. Cryer, and M. Shah, "Shape-from-Shading: A Survey," *IEEE Trans. Pattern Analysis and Machine Intelligence,* vol. 21, no. 8, pp. 690-706, Aug. 1999.
[18] B.K.P Horn and R.W. Sjober, "Calculating the Reflectance Map," *Applied Optics,* vol. 18, pp. 1770-1779, 1979.
[19] M.H. Freeman and C.C. Hull, *Optics,* 11th ed. Elsevier, 2005.
[20] L. Zhang, "Background Reconstruction for Camera-Based Thin-Layer Chromatography," *Optics Express,* vol. 14, pp. 10386-10392, 2006.
[21] W. Rudin, *Principles of Mathematical Analysis,* third ed. McGraw-Hill, 1976.
[22] R. Graham, "An Efficient Algorithm for Determining the Convex Hull of a Finite Point Set," *Information Processing Letters,* vol. 1, pp. 132-133, 1972.
[23] R. Garnett, T. Huegerich, C. Chui, and W.J. He, "A Universal Noise Removal Algorithm with an Impulse Detector," *IEEE Trans. Image Processing,* vol. 14, no. 11, pp. 1747-1754, Nov. 2005.
[24] M. Unser, "Splines: A Perfect Fit for Signal and Image Processing," *IEEE Signal Processing Magazine,* vol. 16, pp. 22-38, Nov. 1999.
[25] Y. Inoue, H. Hori, T. Sakurai, Y. Tokitomo, J. Saito, and T. Misonou, "Measurement of Fluorescence Quantum Yield of Ultraviolet Absorbing Substance Extracted from Red Alga: Porphyra Yezoensis and Its Photothermal Spectroscopy," *Optical Rev.,* vol. 9, pp. 75-87, 2002.
[26] I. Vovk and M. Prosek, "Reproducibility of Densitometric and Image Analyzing Quantitative Evaluation of Thin-Layer Chromatograms," *J. Chromatography A,* vol. 779, pp. 329-336, 1997.
[27] F.T. Chau, T.P. Chan, and J. Wang, "TLCQA: Quantitative Study of Thin-Layer Chromatography," *Bioinformatics,* vol. 14, pp. 540-541, 1998.
[28] L. Zhang and X.G. Lin, "Quantitative Evaluation of Thin-Layer Chromatography with Image Background Estimation Based on Charge-Coupled Device Imaging," *J. Chromatography A,* vol. 1109, pp. 273-278, 2006.

Li Zhang received the BS and MS degrees in signal and information processing from Tsinghua University, Beijing, in 1987 and 1992, respectively. From 1987 to 1989, he taught physics experiments in the Department of Physics at Tsinghua University. In 1992, he joined the faculty of the Department of Electronic Engineering at Tsinghua University. His research interests include image processing, computer vision, pattern recognition, and computer graphics.